

**Solid Electrolyte Interphase:
Can faster formation at lower potentials yield better performance?**

Byron Konstantinos Antonopoulos^a, Christoph Stock^a, Filippo Maglia^a, Harry Ernst Hoster^b

Affiliations:

^a BMW Group, Petuelring 130, 80788 München, Germany

^b Dept. of Chemistry, Lancaster University, Lancaster, LA1 4YB, United Kingdom

Corresponding author: h.hoster@lancaster.ac.uk; +44 7842 831633

Co-Author Addresses: Konstantinos.Antonopoulos@bmw.de, Christoph.Stock@bmw.de,
Filippo.Maglia@bmw.de, H.Hoster@lancaster.ac.uk

Keywords: SEI Formation, Li-ion battery, Pre-Charge, Composite Carbon Electrodes, Cyclic Voltammetry

Highlights:

- The concept of high- and low-potential SEIs applies also on composite electrodes
- The initial high-potential SEI is most relevant for the final SEI properties
- Three formation protocols are demonstrated to improve cell performance
- SEIs grown at higher overpotentials may have more open structures for efficient Li transport
- A slowly formed SEI is not necessarily advantageous for long-term cell performance.

Abstract:

To make a Lithium Ion Battery (LIB) reliably rechargeable over many cycles, its graphite-based negative electrode requires the solid electrolyte interphase (SEI) as a protection layer. The SEI is formed through chemical and particularly electrochemical side reactions of electrolyte components in the first charging cycle(s) after manufacturing of a LIB. The SEI ideally serves two purposes: (i) act as a sieve permeable to Li ions but not to other electrolyte components and (ii) passivate the electrode against further electrolyte decomposition. Core element of conventional SEI formation is a lengthy, low-current galvanostatic charging step, which due to its time consumption contributes heavily to cell manufacturing costs. Here, we report on some non-conventional SEI formation protocols for composite carbon electrodes, inspired by recent experimental findings at smooth model electrodes. Acknowledging that the SEI forms in two main steps, taking place in a high-potential and a low-potential region, respectively, we demonstrate that less time spent in the high-potential region not only makes the process faster but even yields SEIs with superior kinetic properties. We tentatively explain this via basic rules of thin film growth and the role of grain boundaries for ion transport. We also report on the positive influence of multi-frequency potential modulations applied between high-potential and low-potential formation. Given that any new cell chemistry in principle requires its own tailor-made formation process, technologic success of future LIB cells will benefit from a systematic, well-understood toolbox of formation protocols. This paper is meant as a first step, highlighting potentially low-hanging fruits, but also flagging the demand for further systematic studies on model systems and on commercially manufactured cells.

1. Introduction

The first few cycles of a Li-ion battery are referred to as the formation cycles. During these cycles, and in particular during the very first charging, a complex interplay of (electro-)chemical (side) reactions of electrolyte components creates the Solid Electrolyte Interphase (SEI) covering the surface of the negative electrode (anode). For high power/energy densities as well as a long cell lifetime, the SEI should provide good electronic insulation, fast Li^+ conductivity and be stable under both cycling and calendar aging conditions. Core element of conventional SEI formation is a lengthy, low-current galvanostatic charging step, which is supposed to ensure a uniform SEI structure [1–8]. On the other hand, in order to reduce manufacturing costs, formation cycles should be as simple and short as possible. From an industry perspective, these conflicting requirements make it necessary to appropriately adjust the formation protocols in order to compromise between customer expectations in terms of performance and cost [2,3,9–11]. Given that no new cell chemistry is brought to manufacturing level without fine adjustment of multiple electrolyte additives for optimized SEI formation, the formation protocols, i.e., applied currents and potentials, should deserve similar attention and possibly new approaches based on both fundamental and empirical studies.

Matsuoka et al. [12] examined the SEI formation on highly oriented pyrolytic graphite (HOPG), which served as a starting point for another recent study by our group [13,14]. This study identified a two-step formation mechanism with threshold steps occurring at ~ 700 and ~ 400 mV vs. Li/Li^+ . The chemical nature of the SEI compact layer formed at the higher potential step (700 mV) differs significantly from that formed below 400 mV. From potentiostatic experiment current transients we concluded that both SEIs passivate the surface against ongoing SEI formation at the same potential. Hence, the low-potential (carbonate and Li containing) must SEI form through further reduction reaction of the compact high-potential SEI. Electrochemical reactions of solvent molecules only play a minor role in the second step. Under this hypothesis, the chemical and physical properties of the final SEI layer could be affected and therefore controlled by controlling the properties of the high-potential layer.

For this paper, we transferred the insights gained at low surface area carbon electrodes (glassy carbon and highly oriented pyrolytic graphite, HOPG [13,15–19]) to graphite powder based electrodes as used in commercial battery cells. Specifically, we used state-of-the-art composite electrodes in three-electrode half-cells (thus investigated only the graphite half-cell behavior) and commercially established electrolyte. We tested new protocols that make use of the separation of the formation process into a high-potential and a low-potential region, appreciating that those two regions may not be equally “valuable”. A conventional constant-current formation process does not actively manage the time spent in certain potential regions, thus possibly leaving room for improvement. Inspired by a coincidental discovery in previous Electrochemical Impedance Spectroscopy (EIS) experiments at HOPG electrodes, we also tested the influence of superimposed multi-frequency potential modulations on the SEI formation process.

The first part of this paper reports on cyclic voltammetry (CV) results that demonstrate the interplay of the high-potential and the low-potential formation regimes and their overall effect on the subsequently SEI-covered negative electrode. Based on those results, three non-conventional but still commercially applicable formation protocols are tested and benchmarked via their performance in subsequent test cycles. We observe benefits of spending less time in the high-potential regime, which we rationalize based on the principles of electrochemical film growth. Our results do not only confirm the potential technologic relevance of the previously discussed two-step SEI formation mechanism, but provide a springboard for a new formation parameter space to optimize SEI formation. This has the potential to

not only speed-up the formation process in commercial cell manufacturing (where it is one of the most costly production steps [20]) but also to improve the performance of the negative electrode altogether.

2. Experimental

2.1. Setup

Investigated electrodes consisted of MAG-D20 graphite (Hitachi Chemical), 2% wt CMC/SBR binder (Dow Chemical/JSR, respectively) and 2% wt Super-C65 carbon (Timcal) as conductive agent. The demineralized water-containing slurry was coated on 10 μm thick copper foil (Schlenk) with a total loading of $\sim 7 \text{ mg cm}^{-2}$. After pre-drying, calendaring to a porosity of 35% and punching, electrodes were finally dried at 120 $^{\circ}\text{C}$ for 12 h in a vacuum oven ($\sim 10^{-2}$ mbar, Glass Oven B-585 Drying, Büchi Labortechnik). The electrolyte used was EC:EMC 3:7 with 2% wt VC and 1M LiPF_6 (LP572, from BASF). Electrodes were transferred without atmosphere contact into an Argon filled glove box, where they were weighted individually for a first capacity approximation. The other cell components were cleaned with iso-propanol and demineralized water in an ultrasonic bath and then dried at 60 $^{\circ}\text{C}$ before being transferred into the glove box for cell assembly. The glove box contained < 0.1 ppm water and < 3 ppm oxygen. CV experiments were performed in T-shaped ECC-Ref cells with glass fiber separator with 75 μm thickness (both from EL-Cell) soaked with 250 μl of electrolyte. The potentiostat used for CVs was a Bio-Logic VMP 3. All other experiments were performed in Swagelok type T-cells including a Celgard 2325 PP/PE separator soaked with 80 μl of electrolyte. Cells were cycled using a Maccor Series 4200 cycler. In both EL-Cells and Swagelok type cells, counter and reference electrodes were separated and made of Li foil (Alfa Aesar), thus all experiments were performed in three-electrode half-cell configuration. This ensures that any potential changes reflect changes of the graphite working electrode since they are measured against the current-free reference. Any deteriorations of the Li counter electrode, which may well occur, will demand more polarization of that electrode for any given current, but that would not affect the potential determined for the working electrode.

After cell assembly and sealing, cells rested for ~ 3 h before applying external currents or voltages in order to avoid poor electrode wetting.

2.2. Test Protocols

If not otherwise stated, cells were formed with one of the formation protocols described in the following section. The given rates were calculated based on the electrode active mass loading and a specific capacity of 360 mAh g^{-1} . After formation through one of the described protocols, the cells were stored at room temperature for another 5 days. Before being tested, cells were conditioned and the effective capacity was determined. C-rates of testing protocols and state of charge (SOC) calibration are calculated from this effective capacity. All tests were performed in a climate chamber at 25 $^{\circ}\text{C}$. In the sections below, lithiation and delithiation of the electrode will be referred as charging and discharging, respectively.

2.2.1. Formation Protocols

While the formation protocols of commercial cell production lines are kept under lock and key by the manufacturers, we have chosen a “standard formation protocol”, broadly used in laboratories and research production lines, as our benchmark [4–8]. Against that benchmark, we tested three non-conventional formation protocols (see details of all four protocols below). The latter are either inspired by our previous work [13,14] mentioned above or by CV experiments presented below. The specific fundamentals are elucidated in the respective discussion sections. Briefly, combinations of sequential

high- and low-rate galvanostatic and of potentiostatic steps allow us to control the time spent in different potential regions. Furthermore, we demonstrate the effect of small potentiostatic oscillations as part of the SEI formation protocol. Unless otherwise stated, from here on all potentials are given vs. Li/Li⁺.

Figure 1 depicts the standard benchmark and the three non-conventional formation protocols used in this study. The current rate ordinate units are shown as fractional C-rates. The dashed FC-arrows indicate that, after the profile shown in Figure 1, further cycling (FC) is performed.

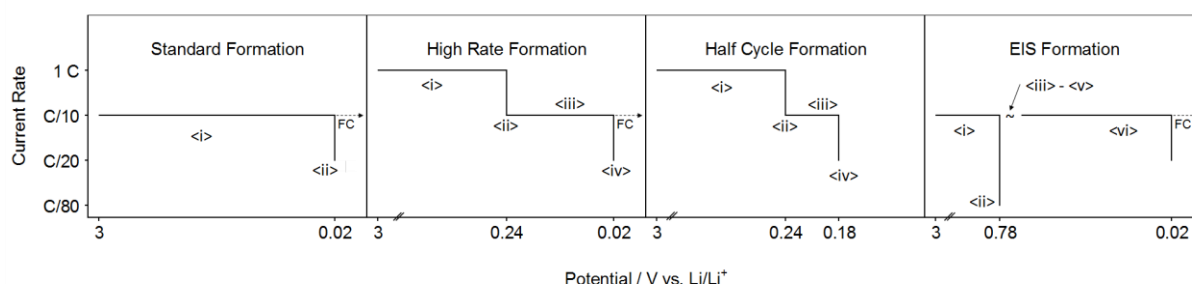


Figure 1: Schematical representation of current profiles of the investigated formation profiles. The vertical bars are potentiostatic steps. The dashed FC-arrow indicates “further cycling” after the presented profiles. For more details see text.

2.2.1.1. Standard Formation Protocol (Benchmark)

<i> charge at 0.1 C until potential ≤ 20 mV; <ii> maintain 20 mV until current ≤ 0.05 C; <iii> discharge at 0.1 C until potential ≥ 1.5 V. <iv> charge at 0.1C to 50% SOC (based on calculated/predicted capacity). Charging and discharging phases were separated by 20 min relaxation phases. Figure 1 depicts only the first charging half-cycle (steps <i> and <ii>, respectively), while the FC-arrow represents the subsequent phases.

2.2.1.2. High-Rate Formation Protocol

Similar to the standard formation but minimizing time spent in “high-potential” region by starting the formation with a higher charging rate: <i> charge at 1 C until potential ≤ 240 mV; <ii> maintain 240 mV until current ≤ 0.1 C; <iii> charge at 0.1 C until potential ≤ 20 mV; <iv> maintain 20 mV until current ≤ 0.05 C; <v> discharge at 0.1 C until potential ≥ 1.5 V; <vi> charge at 0.1 C to 50% SOC. Steps <iii>-<vi> are identical to the standard formation protocol.

2.2.1.3. Half-Cycle Formation Protocol

Similar to the high-rate protocol, but terminating with a constant-voltage phase at 180 mV: <i> charge at 1 C until potential ≤ 240 mV; <ii> maintain 240 mV until current ≤ 0.1 C; <iii> charge at 0.1 C until potential ≤ 180 mV. <iv> maintain 180 mV until current ≤ 0.05 C.

2.2.1.4. EIS Formation Protocol

Makes use of a side-effect of potential modulations for EIS (electrochemical impedance spectroscopy, using the Bio-Logic potentiostat): <i> charge at 0.1 C until potential ≤ 780 mV; <ii> maintain 780 mV until current ≤ 32 μ A (\sim C/80); <iii> open circuit potential (OCP) for 30 min; <iv> EIS cycle: potentiostatic modulation with 10 mV amplitude around OCP, using 50 logarithmically distributed frequencies in range 500 kHz...0.1 Hz; <v> repeat EIS cycle 50 times; <vi> transfer cell to the Maccor cycler and apply Standard Formation Protocol.

2.2.2. Conditioning, SOC Calculation

After applying the formation protocols and before testing the electrode performance, cells were checked for quality and the nominal capacities were re-determined. For that, the cells were charged

and discharged similar to the Standard Formation Protocol for ~3.75 cycles: <i> charge at 0.1 C until potential ≤ 20 mV; <ii> maintain 20 mV until current ≤ 0.05 C; <iii> discharge at 0.1 C until potential ≥ 1.5 V; <iv> repeat 4 times. Charging and discharging phases were separated by 20 min relaxation phases. The last discharge capacity was used for re-determination of C-rates and calibration of the SOC scale for the testing protocols.

2.2.3. Testing Protocols

2.2.3.1. Cycle Aging Test at 1 C

<i> charge at 1 C until potential ≤ 20 mV; <ii> maintain 20 mV until current ≤ 0.05 C; <iii> relax for 20 min; <iv> discharge at 1 C until potential ≥ 1.5 V; <v> go back to <i>.

2.2.3.1. Variable Rate (0.33...5 C) Discharge Test

<i> charge at 0.1 C until potential ≤ 20 mV; <ii> maintain 20 mV until current ≤ 0.05 C; <iii> relax for 20 min; <iv> discharge at x C until potential ≥ 1.5 V (x = 0.33, 0.5, 1, 2, 3, 5, 0.1); <v> relax for 20 min; <vi> repeat three times for every x, then go to next x in list.

2.2.3.2. OCP vs. SOC Profiles

Charge/discharge cycles interrupted at certain SOC values for OCP reading: <i> charge at 0.1 C until potential ≤ 20 mV, interrupted at SOC values 10, 30, 50, 70 and 90% for precise OCP reading; <ii> maintain 20 mV until current ≤ 0.05 C; <iii> relax for 20 min; <iv> discharge at 0.1 C until potential ≥ 1.5 V, interrupted at SOC values 90, 70, 50, 30 and 10% for OCP reading.

OCP reading steps: wait for stable open circuit potential ($dOCP/dt < 0.1$ mV s⁻¹), but no longer than 60 min; then register OCP and continue with charge/discharge. The two OCP values from discharging and charging directions were averaged for each SOC.

All experiments were reproduced with three different cells to avoid conclusions based on random findings. The error bars in some of the diagrams below reflect standard deviations within those cohorts.

3. Results and Discussion

3.1. Cyclic Voltammetry Experiments

Cyclic voltammetry (CV) is less commonly used for composite electrodes than galvanostatic methods. However, at sufficiently slow scan rates, CV scans nicely show onset and possible passivation potentials of electrochemical reactions. For an HOPG electrode, Matsuoka et al. obtained slow SEI formation CVs in a similar electrolyte as we use here (yet different solvent ratio), and identified two major reaction steps at ~400 and ~700 mV [12]. These two steps, which correspond to two different SEI formation stages, may shift by several 100 mV at other graphite materials [13,21].

To identify the position of potential steps and their relative magnitude on our electrodes, we performed formation CVs on freshly built cells. Starting at OCP (~3 V), we went down to 20 mV at a rate of 20 and 10 μ V s⁻¹ and back up to 1.5 V. Figure 2 shows the high-potential regions of the respective first negative going scans. Although not perfectly sharp, a first distinct reduction reaction is apparent in a negative peak/shoulder (α) at ~920 mV. The local current minimum (β) at 780 mV corresponds to the passivation potential at which the reaction is almost fully completed and further (secondary) mechanisms (γ) start taking place. This onset potential is used and discussed in the later part of this work.

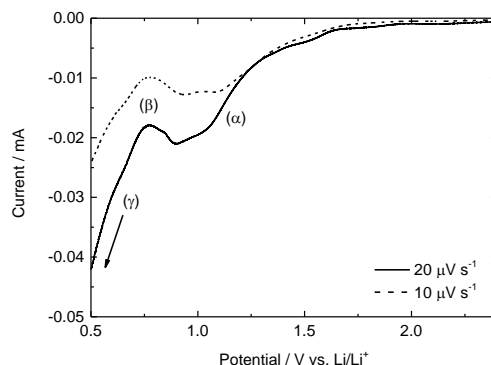


Figure 2: High-potential region of SEI formation CVs using indicated scan rates. Full cycles are presented in the supporting information. Peak assignment: see section 3.1.

Since both scan rates produced similar results, the remaining part of this section is restricted to $20 \mu\text{V s}^{-1}$ results for the sake of brevity. In the following, the results of two related experiments will demonstrate that the time spent in the high-potential region makes a difference for the intercalation kinetics in the first scan.

Experiment 1. Figure 3a shows the potential region $< 300 \text{ mV}$ of first and third scan, in continuation of the CV plotted in Figure 2. Table 1 lists all distinguishable peak potentials. The first and third cycle differ during the intercalation sweep (negative currents) at $< 210 \text{ mV}$: the first scan does not exhibit separable current peaks and the current keeps increasing as the scan reaches the lower potential limit. On the other hand, the third scan shows the typical graphite intercalation features, including a current drop at potentials below 50 mV due to Li^+ saturation in graphite [21–23]. The third scan exhibits three negative peaks (labelled (i), (ii), (iii)) at 179, 131 and 67 mV ; the a shoulder at $\sim 48 \text{ mV}$ could be a fourth intercalation step. The small current increase at $\sim 30 \text{ mV}$ could be attributed to Li plating.

The deintercalation currents in the subsequent positive going scans split into three peaks (labelled (v), (vi), (vii)). Peak (v) is much smaller in the first cycle, but (apart from a 3 mV shift) peaks (vi) and (vii) are virtually identical for 1st and 3rd cycle (see Table 1). Those peaks reflect the known deintercalation steps of graphite [22,23]. Their presence even in the first scan demonstrates that the negative currents in the first scan must reflect Li^+ intercalation, albeit not at the potentials of peaks (i)-(iii) but shifted to more negative potentials. This causes the fourth intercalation step (shoulder in 3rd scan) to be of minor occurrence in the 1st scan, therefore the corresponding deintercalation peak (v) is small. Our chosen scan rate of $20 \mu\text{V s}^{-1}$ is comparably low [12], hence the peak shifts are unlikely to be experimental artifacts but will rather reflect additional kinetic barriers for Li intercalation during this first negative polarization [24]. In this picture, the polarization to very low potentials ($< 100 \text{ mV}$) removes at least part of these initially inhibiting barriers, allowing inconspicuous Li^+ deintercalation in the subsequent reversed potential sweep and separated intercalation and deintercalation peaks in all following cycles.

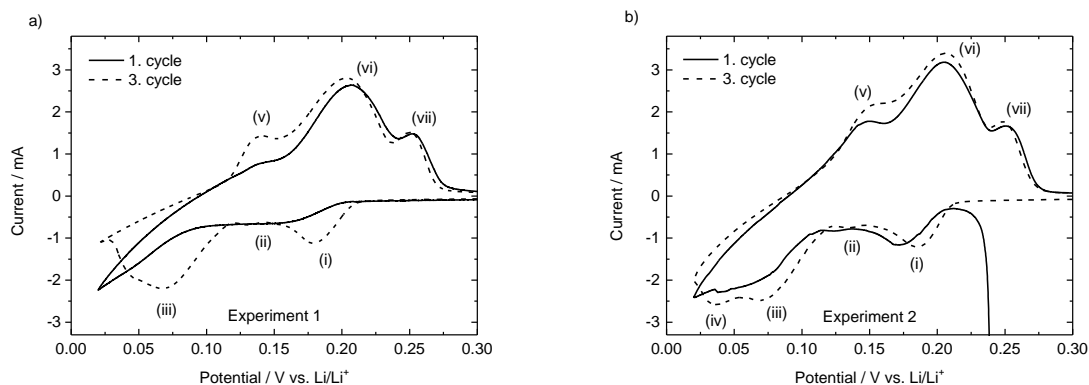


Figure 3: Effects of spending more or less time in the high-potential region on (de-)intercalation CV features. Solid and dashed lines indicate the first and third scans, respectively, of graphite electrodes in the range 20 mV...1.5 V. First scan starts from OCP in negative direction (see Figure 2) a) Scan rate $20 \mu\text{V s}^{-1}$; b) Scan started with 5 mV s^{-1} down to 240 mV, then continued with $20 \mu\text{V s}^{-1}$. Potential positions of numbered peaks are listed in Table 1.

Experiment 2. Given that no such first-intercalation inhibitions were reported on similar electrodes in previous works where higher formation scan rates were used [25], the long time (~ 13 h) spent in the higher potential region ($\sim 1.2 \dots 0.24$ V) is a likely reason for our observation. This is confirmed by the results of experiment 2, presented in Figure 3b, which shows very similar data as in Figure 3a, but without a “legacy” as produced by the 13h spent at high potential. Here, the initial potential scan from OCP down to 240 mV was performed at 5 mV s^{-1} , which reduced the time spent in the $1.2 \dots 0.24$ V region to only ~ 3 min.

At such a high scan rate, the electrolyte reduction reactions are driven into diffusion limited regime, which limits the current drawn from the potentiostat and the total charge spent in the high-potential reaction. After reaching 240 mV (see steep current step in Figure 3b: currents at 5 mV s^{-1} are out of plotted range), the scan rate is reduced to (and kept at) $20 \mu\text{V s}^{-1}$ for the following cycles between 20 mV and 1.5 V.

In contrast to experiment 1, the shorter time spent in the high-potential regime reduced the kinetic inhibition of Li intercalation in the first negative going scan. This is apparent from the much more pronounced peaks even in the first cycle of experiment 2 (see Table 1 for peak positions), in particular peak (i) (which has the earliest onset potential). Unlike in experiment 1, all relevant features, including total charge, position of lithiation peaks (i) and (ii) (at ~ 180 and ~ 130 mV), as well as the broad lithiation peak starting at ~ 110 mV, and overall slopes of the current profiles are similar for 1st and 3rd cycle. Only differences in the first intercalation scan are negative shifts of peaks (i)-(iii) by ~ 13 mV and a not fully developed peak 4, all indicative for a minor kinetic inhibition. The deintercalation peaks (v)-(vii) are at the same positions but slightly larger in the third than in the first cycle, reflecting lower Li uptake in the first cycle but otherwise similar conditions.

Apart from those effects on the first-cycle (de-)intercalation features, the time spent in the high-potential region also influences later cycles. This is obvious when comparing the respective third cycle profiles in Figure 3a and b. E.g., peak (iv) (at 50 mV) in Figure 3b only appears as a “shoulder” in Figure 3a. Since the three-electrode setup excludes contributions from other electrodes, we tentatively assign these differences to different SEIs formed depending on how much formation time is allowed in the high-potential region. The sharper and higher (de-)intercalation peaks observed in experiment 2 indicate that formation protocols with less time spent at higher potentials may produce SEIs with lower Li^+ transport barriers. Those include ionic movement and Li^+ desolvation.

Table 1: Potentials of CV peak maxima of the slopes presented in Figure 3, given in mV vs. Li/Li⁺.

Exp.	Scan Rate		Intercalation Maxima				Deintercalation Maxima		
			(i)	(ii)	(iii)	(iv)	(v)	(vi)	(vii)
1	20 $\mu\text{V s}^{-1}$	1. Cycle	-	-	-	-	~144	207	252
		3. Cycle	179	131	67	-	141	204	250
2	5000 / 20 $\mu\text{V s}^{-1}$	1. Cycle	171	124	~55	-	149	205	250
		3. Cycle	185	135	70	36	~155	206	249

3.2. High-Rate Formation Protocol

Our findings in the previous section indicate advantages of spending less time in the high-potential region during SEI formation. This provides the starting point for our attempt to accelerate the formation and improve the properties of the SEI at the same time. Since formation of cells in series production is performed galvanostatically for practical reasons, we designed a specific galvanostatic protocol that causes potential profiles very similar to the dynamic CV formation of experiment 2 in the previous section (cf. Figure 3b). This “high-rate formation protocol” differs from the standard formation protocol in one aspect: instead of a galvanostatic charge at 0.1 C all the way down to 20 mV, the cell is charged at 1 C down to 240 mV. The 10-fold higher current makes the galvanostat impose a faster negative potential sweep on the working electrode. The potential of 240 mV is kept until the current drops to 0.1 C, which is then kept galvanostatically until the potential reaches 20 mV (see Figure 1b and related explanation for more details). Note that the potentiostatic part of this protocol is a “relaxation” step during which the current only gets smaller. In contrast to abrupt potentiostatic steps, this is technically manageable even for large capacity electrodes, whilst the time spent in the high-potential region is still short.

For the high-rate and the standard protocol, Figure 4 shows the resulting potential profiles and the relative SOC_s during the respective formation processes. The relative capacities are calculated by normalizing the integrated charges to the actual electrode capacity (determined in the later conditioning step, see experimental section), and is therefore given as SOC. As expected, due to the high current, the potential of the high-rate cell drops to the step potential of 240 mV within < 3 min. In the subsequent potentiostatic step at 240 mV, the current drops to < 0.1 C in < 5 min, indicating rather quick self-passivation of the electrolyte reduction process. Apart from those differences in the beginning, the potential profiles produced by both protocols have similar shapes. The plateaus (i), (iii) and (iv) in Figure 4 are the galvanostatic representatives of the respectively numbered CV peaks in Figure 3, meaning that the currents are dominated by Li intercalation, with some (capacity-wise minor) superimposed contributions from SEI formation. The three plateaus during the “high-rate formation” are higher by 10-20 mV than those of the standard formation, reflecting a lower lithiation overpotential achieved through the high-rate as compared to the standard protocol.

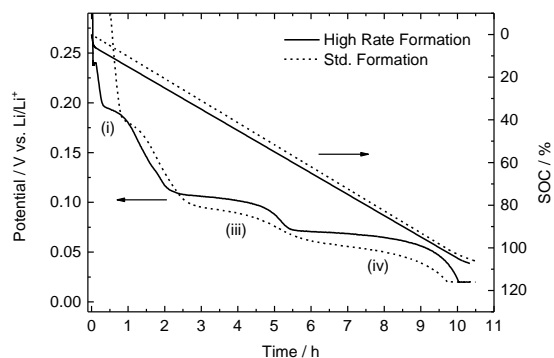


Figure 4: Potential and normalized charge profiles during the first lithiation half-cycle of a high-rate formation protocol. For comparison, the profile during a standard formation protocol is shown. Plateaus correspond to respective lithiation peaks in Figure 3 and Table 1.

Figure 5a demonstrates that also the barriers for subsequent delithiation are lower after the high-rate than after the standard formation protocol. The potential profiles from the rate discharge test show the most pronounced differences for higher C-rates: at 2 C, the charging overpotential is lower by more than 100 mV for the “high-rate” than for the “standard” SEI. Note that the OCP values from OCP/SOC show (thermodynamically) no difference for the two formation protocols, underlining that the different protocols only affect the cell kinetics combination. There is consensus that the major cause for overpotentials at the graphite negative electrode is the low Li^+ conductivity of the SEI compact layer [26]. Since the counter electrode is irrelevant in our three-electrode half-cell setup, we conclude that the high-rate formation protocol forms an SEI with better Li^+ conductivity and/or desolvation kinetics as compared to the standard protocol. Using 50% SOC as a comparison point, both 1 C and 2 C slopes indicate a reduction of effective SEI resistance by 27%.

To exclude the possibility that this kinetic improvement is offset by inferior long-term performance/stability, we performed cycle aging tests. Discharge capacities and coulombic efficiencies during 100 cycles are presented in Figure 5b. The capacity is very stable at $> 360 \text{ mAh g}^{-1}$ over the whole test duration. The error bars are nearly of constant height indicating a similar aging of the three tested cells. The coulombic efficiency rises to $> 99.9\%$ with negligible error bars until cycle 20, where a larger scatter in the values obtained for the cells can be observed. Overall, Figure 5b confirms very good cycle behavior of the cells that were initiated via the high-rate formation protocol, indistinguishable from the normally formed cells (presented in SI).

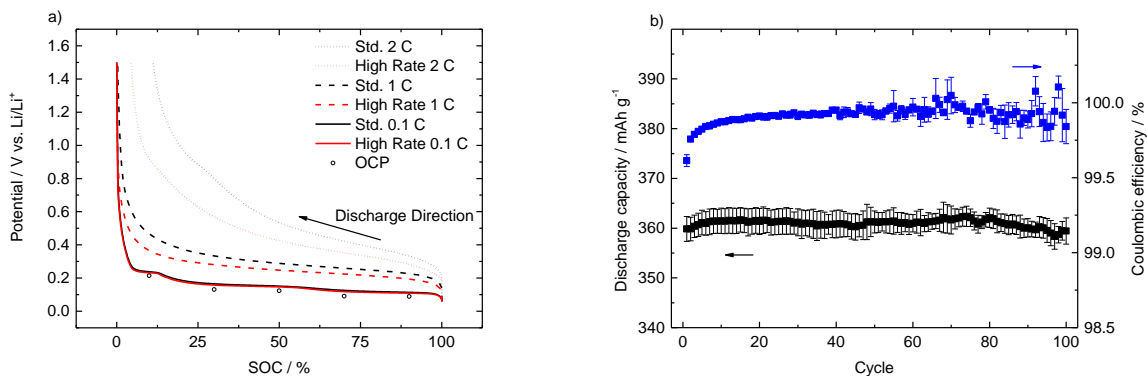


Figure 5: a) Rate discharge potential profiles at different current rates after applying the standard or high-rate formation protocol; circles indicate the OCP at respective SOC. b) Discharge capacity and coulombic efficiency of graphite electrodes pretreated with the high-rate formation protocol during a cycle aging test.

3.3. Half-Cycle Formation Protocol

As mentioned in the introduction, a key driver to try and re-think the formation process is the need to save time, i.e., saving costs in the cell supply chain. The high-rate formation protocol just demonstrated time savings via an initially high charge rate that drives the potential of the graphite electrode rapidly down to 240 mV. Apart from saving irreversible charge losses this seemed to have even improved the kinetic properties of the resulting SEI.

Appreciating that the high-rate protocol brought the formation time from > 24 h down to 11 h (see Figure 4), further time and irreversible losses could be saved by restricting the formation process to the truly relevant potential windows and by skipping the final charge/discharge cycle. Our previous experiments at HOPG surfaces confirmed previous findings that SEI formation predominantly takes place in two steps, with the second step being largely complete in the potential region > 200 mV [13]. Hence, polarizing the electrode to potentials below 200 mV might not be necessary for full passivation or long-term stability. However, Figure 4 illustrates that > 9 h of the formation process are spent in that very region.

The half-cycle formation protocol (Figure 1c) thus stops the controlled passivation process at 180 mV instead of 20 mV. In detail: similar to the high-rate protocol, the cell is charged at 1 C until the negative electrode reaches 240 mV, where the potential is held to let the current relax down to 0.1 C. The 0.1 C current is then kept until 180 mV are reached. 180 mV are then kept until the current reaches < 0.05 C.

As illustrated in Figure 6, this process is finished after 1.2 h, including the 11 min final potentiostatic step at 180 mV until 0.05 C are reached. After that, only the OCP is recorded. The half-cycle protocol ends at the end of the first plateau (~190 mV), which (similar to peak (i) in the CV in Figure 3) reflects the first stage of graphite lithiation. This is supported by the subsequent OCP value of 213 mV, which according to Figure 5b belongs to about 10% SOC.

In the following we will test whether bringing the formation time from 27 h (standard formation plus subsequent full cycle) down to 1.2 h comes with poorer rate performance or long-term stability.

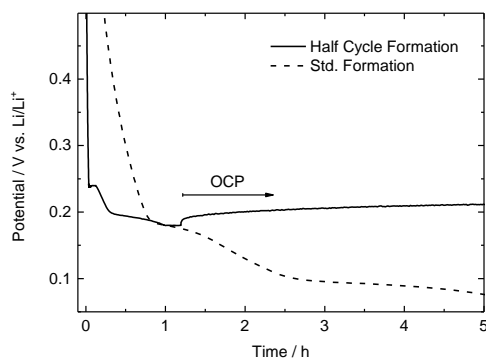


Figure 6: Potential profile during a half-cycle formation protocol. The active operation is completed after 1.2 h, after which OCP is obtained. For comparison, the profile during a standard formation protocol is shown.

Figure 7a (rate discharge test) shows that, for the same C-rates (0.1, 1 and 2 C), the potential profiles of the cells after half-cycle formation are very similar to those obtained for cells after high-rate formation (Figure 5a). Accordingly, the amounts by which the discharge overpotentials are reduced are very similar, too, which confirms the beneficial effect of spending less time in the high-potential region. The matching OCP values confirm that also this SEI formation protocol does not affect the thermodynamic electrode properties.

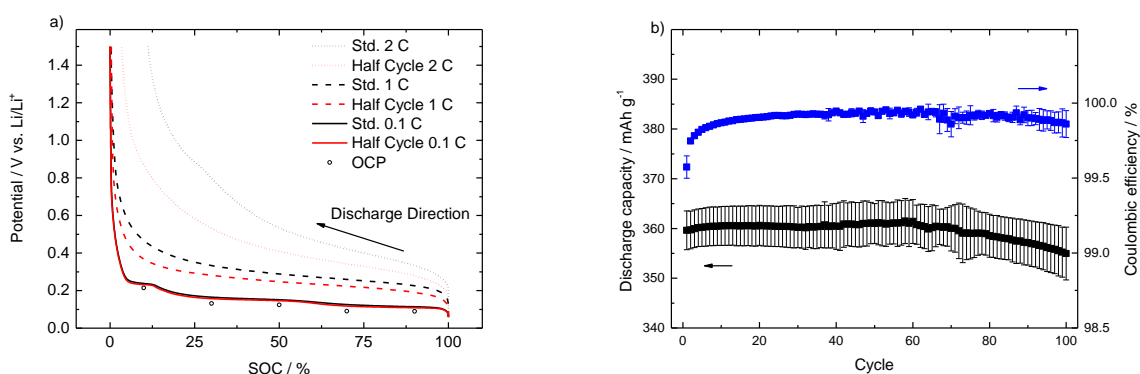


Figure 7: a) Rate discharge potential profiles at different current rates after applying the standard or half-cycle formation protocol; circles indicate the OCP at respective SOC. b) Discharge capacity and coulombic efficiency of graphite electrodes pretreated with the half-cycle formation protocol during a cycle aging test.

Cycle aging tests of the cells after the half-cycle formation protocol (Figure 7b) show a behavior very similar to the one observed for the high-rate protocol (Figure 5b). The capacity is initially at 360 mAh g^{-1} . The respective error bar height is constant, indicating that the cells behave similarly (note that the error bars mainly reflect systematic errors of inaccurate active masses). This is underlined by the high efficiency $> 99.9\%$ and its virtually missing error bars. Discharge capacity and coulombic efficiency start dropping slightly after the 70th cycle, which leads to a loss of capacity of 3% after the 100 cycles. Here, the time saving half-cycle protocol may indeed exhibit a small weakness as compared to high-rate or standard protocol (as far as laboratory type three-electrode half-cells can tell). Comparing the coulombic efficiencies in Figures 5a and 7a, however, it is clear that the additional hours spent in the potential region $< 180 \text{ mV}$ do not visibly reduce the number of “starting” cycles required to reach $> 99.9\%$.

The very time saving half-cycle protocol deserves further studies beyond laboratory three-electrode half-cells: industrially manufactured full cells may behave totally different (see also supporting

information) [27,28]. Those studies will have to quantify the actual gain in performance and durability that are gained in the additional hours of the longer formation protocols.

3.4. EIS Formation Protocol

This third alternative formation protocol is a first step beyond the rather smooth combinations of galvanostatic and potentiostatic periods. Here, we provide preliminary evidence that a frequency stimulation (as used in electrochemical impedance spectroscopy, EIS), applied during the formation process, can also improve the kinetic properties of the SEI. Testing of this approach was inspired by a rather coincidental discovery during a model study on SEI formation on HOPG (to be published separately [14]). Previous attempts with a similar approach were published by Wang et al. [29]. In their work, a continuous charging current was supplemented by current pulses throughout the whole first charging half-cycle. However, cycling results were incoherent and strongly depended on the amplitude of the overlapping current pulses.

The EIS formation protocol (see Figure 1d) starts and ends with the standard formation protocol. However, after reaching 780 mV (see “ β ” in Figure 2), where in our picture the high-potential SEI is formed, this high-potential SEI is subject to “AC treatment” (50 EIS spectra at 10 mV amplitude and 50 logarithmically distributed frequencies in range 500 kHz...0.1 Hz). After that, galvanostatic charging down to 20 mV is continued at 0.1 C. Prior to the EIS treatment, the potential of 780 mV is held to allow the current to relax down to C/80. (See SI for the recorded impedance spectra; note that those were not recorded at any thermodynamically well-defined potential)

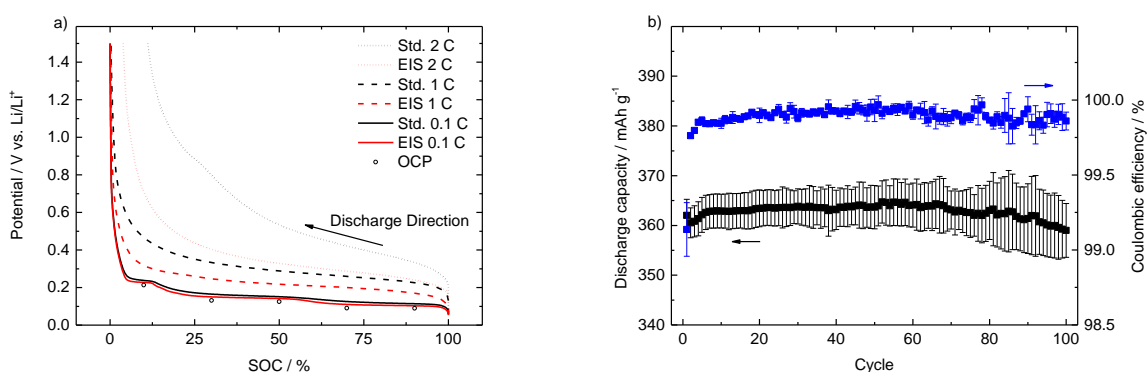


Figure 8: a) Rate discharge potential profiles at different current rates after applying the standard or EIS formation protocol; circles indicate the OCP at respective SOC. b) Discharge capacity and coulombic efficiency of graphite electrodes pretreated with the EIS formation protocol during a cycle aging test.

Figure 8a compares the rate performance of the resulting electrode to that achieved after the standard formation protocol at 0.1, 1 and 2 C. Again, the OCP values are not affected by the alternative treatment. The rate performance, however, shows improvements: using the overpotentials of the 1 C and 2 C profile at 50% SOC as benchmark points, the SEI resistance is reduced by 45-50%. Those improvements did not occur when the potentiostatic period at 780 mV was just followed by a long OCP phase without the additional AC excitation. Hence, the EIS treatment itself must have made the difference.

The high-potential SEI as formed at 780 mV and above is a precursor for the subsequent low-potential SEI formation, which (as discussed in the previous sections) predominantly occurs in the potential window 240...180 mV. Since the AC excitation is applied around OCP, no net currents could feed any ongoing electrochemical reaction of the SEI. Given that any chemical reaction should also have happened in the control experiment without EIS, we are left with the option that the AC excitation

causes physical or structural changes to the high-potential SEI. As a working hypothesis, we suggest a re-orientation of the SEI components with respect to the graphite surface in response to the alternating near-surface electric field. If such a re-orientation includes disentangling of polymers, one could imagine a scenario where the subsequent low-potential reactions consolidate a structure that provides more/wider/better oriented/less tortuous channels for Li transport. Clearly, a better understanding and an efficient exploitation of the observed phenomena require further studies including more specific AC excitations in combination with spectroscopic analyses of the resulting SEI layers, which would be beyond the scope of this paper.

The cycle performance tests results in profiles similar to those presented above. The coulombic efficiency quickly reaches > 99.9% with almost no error bars. The discharge capacity shows the possibility of extracting > 360 mAh g⁻¹. The error bars are constant, indicating a similar cell behavior within the cohort. After the 60th cycle the discharge capacity starts dropping slightly while the respective error bars grow. This is coherent with the observed drop of coulombic efficiency to ~99.8%. Considering the stable discharge capacity in the cycles 20...50 as a reference, the cell suffers from a capacity loss of 1.5% after 100 cycles. Here, the growth of the error bars in principle indicates a scattering of the single cell capacities, though a capacity fade is presumed as well.

3.5. Discussion

Our results underline that the two-step SEI formation, distinguishing a high-potential and a low-potential region, is more than an academic concept and can be utilized to tune SEI properties. Cyclic voltammetry as initial SEI forming treatment showed sharper lithiation peaks if the high-potential region from OCP down to 240 mV was passed at higher rate in the very first scan. The (technically more relevant) galvanostatic high-rate and half-cycle protocols used initially high currents to make the galvanostat quickly drive the potential down to 240 mV and then continued charging the cells more slowly. Mass transport limitations allow for the “rushing” through the high-potential region without uncontrollably large currents. In comparison to the standard protocol, where a lower current keeps the electrode in the higher potential region for longer, both alternative protocols yielded to SEIs that provided the graphite electrodes with better rate capabilities.

Without direct information about structure and chemistry of the SEI after the various formation processes, we tentatively rationalize the observed behavior based on the principles of electrochemical film deposition. The electrochemical reactions contributing to SEI formation are multi-step reduction processes; hence the attempt of growing most of the SEI at less positive potentials implies growth at higher overpotentials. This comes with a higher nucleation rate and thus a higher granularity of the film [30,31]. Additionally, less positive potentials facilitate reactions with lower onset potentials, further increasing the film inhomogeneity. Grain boundaries are considered essential for ion transport at the positive electrode: For instance, Noh et al. reported that Li⁺ moves faster along grain boundaries, thus leading to smaller inner-particle concentration gradients [32–34]. Going back to the negative electrodes, Li⁺ has to strip off its solvation shell at the SEI compact layer in order to move through the SEI compact layer minerals at the electrode surface before intercalating [35–37]. Adapting the grain boundary concept from the positive electrode materials, grain and phase boundaries of inorganic species in the compact layer could act as ion channels, similar to the concepts discussed by Zhang et al. [38]. Li⁺ moves predominantly along the phase and grain boundaries instead of through the bulk. The existence of ion channels would be compatible with the SEI microphase model, which was early proposed by Peled et al. [39] and diffusivity results by Bhattacharya et al. [40].

In this picture, the higher current and concomitantly higher SEI growth rate in the high-potential region, in combination with subsequent growth at higher overpotentials over longer periods in the low-potential region would create a more granular, open SEI with more efficient ion channels. Longer &

slower growth at higher potentials, on the other hand, creates a smoother, less permeable SEI. A slow formation rate is probably only advantageous for the formation of the final compact layer, to ensure chemical passivation and long term stability.

More clarity must be provided through surface sensitive microscopy and spectroscopy on SEIs formed according to the various protocols, possibly in combination with model studies on Li^+ conductivity of different ex-situ deposited SEI layers (e.g. Li_2CO_3) with varying crystallite sizes. Ex-situ and in-situ structure analyses will also be the only way to get some understanding about the rather unexpected effects of applying 10 mV multi-frequency excitations between the high-potential and low-potential SEI formation periods, i.e., the “EIS formation protocol”.

Accepting the positive effect of the three alternative formation protocols on the Li transport kinetics of the resulting SEI, one should still highlight that all protocols yielded cells with similar cycle aging characteristics (apart from some nuances). This is in contrast to the widely accepted rule that the SEI should be formed with slow rates to make it chemically and physically uniform [2,3]. Uniformity shall warrant a homogenous current distribution, which in turn guarantees better long-term stability.

Given the relevance of the SEI as one of the main contributors to the internal resistance of a full cell [41], we expect our findings to trigger further studies. The three-electrode half-cells allowed us to selectively study SEI formation on graphite, without overpotentials occurring at the counter electrode tampering with our working electrode potentials during formation and subsequent experiments. Experiments at such cells, however, cannot replace similar studies at technical full cells but are rather their starting point:

Firstly, the cycle performances of half cells are not directly comparable to those of full cells. Capacity fading after > 70 cycles could reflect degradation of the graphite working electrode but also dendrite formation at the Li counter electrode. Our cycle aging tests thus only allow us to conclude that none of the SEI formation protocols deteriorated the subsequent cycle aging in a way that would flag a principal problem of that protocol. They do not allow conclusions about formation protocols and the resulting longer-term cyclability. Secondly, we can't know what effects our alternative formation protocols would have on technical cathode materials. In summary, the work presented here motivates and informs similar experiments with commercial full cells, ideally in combination with further analytical methods including gas evolution analyses.

4. Conclusion

Inspired by previous findings at smooth carbon model electrodes we explored new protocols to form the solid electrolyte interphase (SEI) on carbon composite electrodes in a three-electrode setup, as they are used as negative electrodes in commercial lithium ion batteries. Main motivation is to make the formation process shorter (for cost reasons) whilst maintaining or even improving the quality of the SEI.

Cyclic voltammetry showed that also for carbon composite electrodes the formation process splits into two potential regions. The electrochemical reduction reactions that contribute to SEI formation predominantly take place in the range 1.2...0.78 V vs. Li/Li^+ (high-potential region) and 0.24...0.18 V vs. Li/Li^+ (low-potential region). Driving the potential quickly through the high-potential region and down to the onset of the low-potential region showed much sharper Li intercalation peaks even during the first reduction sweep. We interpreted that as an indicator for better Li^+ conductivity of an SEI formed predominantly at potentials < 0.24 V vs. Li/Li^+ .

Based on these insights, we tested two advanced SEI formation protocols that combine galvanostatic and potentiostatic steps and minimize “high-potential” SEI components. In subsequent galvanostatic charge/discharge cycles, the resulting electrodes showed clearly superior rate capabilities, in agreement with the expectations from the CV experiments. There was even evidence that the potential region 180...20 mV vs. Li/Li⁺ could potentially be skipped, which would save hours of time in a commercial formation process.

Based on the principles of electrochemical film growth, SEI formation at lower potentials (hence, higher overpotentials for involved electrochemical reduction steps) may occur at higher nucleation rate, thus creating more and smaller grains with more overall grain boundary regions. Such a morphology may provide more channels for Li⁺ transport, in analogy to the known enhanced Li⁺ transport along grain boundaries in the particles of positive electrode materials

A third advanced formation protocol was based on some recent empirical findings for HOPG electrodes: applying 10mV multi-frequency excitations between the high-potential and low-potential SEI formation periods, using an Electrochemical Impedance Spectroscopy instrument (“EIS formation protocol”). Similar to the other two unconventional protocols, the resulting SEI showed superior rate capability. Whilst we could only present this observation as a preliminary empirical finding, we tentatively proposed an orienting/alignment effect of the local AC field on the precursor SEI (from the high-potential region) that may eventually lead to a less entangled, more open structure to be “cured” in the subsequent low-potential region.

The presented approaches and models may inspire a new field of SEI optimization research in defined cell chemistries. Given that all three approaches seem to warrant a faster (=cheaper) formation process and/or an SEI with better Li transport properties (=more power), they should be tested at commercially produced full cells as soon as possible.

5. Acknowledgements

We acknowledge the providing of electrodes and partial cell building and testing by the technical laboratory of the BMW Group. Furthermore we would like to thank Prof. Brett Lucht (Rhode Island University) for fruitful discussions on the topic of ion channels in the SEI.

6. References

- [1] F.M. Kindermann, P.J. Osswald, S. Klink, G. Ehlert, J. Schuster, A. Noel, S.V. Erhard, W. Schuhmann, A. Jossen, Measurements of lithium-ion concentration equilibration processes inside graphite electrodes, *Journal of Power Sources* 342 (2017) 638–643.
- [2] J.Q. Xu, Dynamic Formation Protocol for Lithium-Ion Battery, US20150060290 (2015), Xu, Jeff Qiang.
- [3] P.-C.J. Chiang, M.-S. Wu, J.-C. Lin, A Novel Dual-Current Formation Process for Advanced Lithium-Ion Batteries, *Electrochem. Solid-State Lett.* 8 (2005) A423.
- [4] Z. Chen, J.R. Dahn, Improving the Capacity Retention of LiCoO₂ Cycled to 4.5 V by Heat-Treatment, *Electrochem. Solid-State Lett.* 7 (2004) A11-A14.
- [5] M.A. McArthur, S. Trussler, Dahn JR, In Situ Investigations of SEI Layer Growth on Electrode Materials for Lithium-Ion Batteries Using Spectroscopic Ellipsometry, *J. Electrochem. Soc.* 159 (2012) A198-A207.
- [6] R. Jung, M. Metzger, F. Maglia, C. Stinner, H.A. Gasteiger, Oxygen Release and Its Effect on the Cycling Stability of LiNi_x Mn_y Co_z O₂ (NMC) Cathode Materials for Li-Ion Batteries, *J. Electrochem. Soc.* 164 (2017) A1361-A1377.

- [7] R. Jung, M. Metzger, D. Haering, S. Solchenbach, C. Marino, N. Tsiouvaras, C. Stinner, H.A. Gasteiger, Consumption of Fluoroethylene Carbonate (FEC) on Si-C Composite Electrodes for Li-Ion Batteries, *J. Electrochem. Soc.* 163 (2016) A1705-A1716.
- [8] S. Klink, W. Schuhmann, F. La Mantia, Vertical Distribution of Overpotentials and Irreversible Charge Losses in Lithium Ion Battery Electrodes, *ChemSusChem* 7 (2014) 2159–2166.
- [9] P. Verma, P. Maire, P. Novak, A review of the features and analyses of the solid electrolyte interphase in Li-ion batteries, *Electrochimica Acta* 55 (2010) 6332–6341.
- [10] M. Winter, W.K. Appel, B. Evers, T. Hodal, K.-C. Möller, I. Schneider, M. Wachtler, M.R. Wagner, G.H. Wroldnigg, J.O. Besenhard, Studies on the Anode/Electrolyte Interface in Lithium Ion Batteries, *Monatshefte fuer Chemie/Chemical Monthly* 132 (2001) 473–486.
- [11] M.B. Pinson, M.Z. Bazant, Theory of SEI Formation in Rechargeable Batteries: Capacity Fade, Accelerated Aging and Lifetime Prediction, *J. Electrochem. Soc.* 160 (2013) A243-A250.
- [12] O. Matsuoka, A. Hiwara, T. Omi, M. Toriida, T. Hayashi, C. Tanaka, Y. Saito, T. Ishida, H. Tan, S.S. Ono, others, Ultra-thin passivating film induced by vinylene carbonate on highly oriented pyrolytic graphite negative electrode in lithium-ion cell, *Journal of Power Sources* 108 (2002) 128–138.
- [13] B.K. Antonopoulos, F. Maglia, F. Schmidt-Stein, H.E. Hoster, Chemical, Electrochemical and Physical Dependencies of the Solid Electrolyte Interphase on the Formation Potential, in submission.
- [14] B.K. Antonopoulos, A.-C. Gentschev, F. Maglia, H.E. Hoster, The Dynamic Impedance Properties of Solid Electrolyte Interphase on HOPG, Manuscript in preparation.
- [15] M. Tang, S. Lu, J. Newman, Experimental and Theoretical Investigation of Solid-Electrolyte-Interphase Formation Mechanisms on Glassy Carbon, *J. Electrochem. Soc.* 159 (2012) A1775-A1785.
- [16] M. Tang, K. Miyazaki, T. Abe, J. Newman, Effect of Graphite Orientation and Lithium Salt on Electronic Passivation of Highly Oriented Pyrolytic Graphite, *J. Electrochem. Soc.* 159 (2012) A634-A641.
- [17] M. Tang, J. Newman, Electrochemical Characterization of SEI-Type Passivating Films Using Redox Shuttles, *J. Electrochem. Soc.* 158 (2011) A530-A536.
- [18] M. Tang, J. Newman, Transient Characterization of Solid-Electrolyte-Interphase Using Ferrocene, *J. Electrochem. Soc.* 159 (2012) A281-A289.
- [19] M. Tang, J. Newman, Why is the Solid-Electrolyte-Interphase Selective? Through-Film Ferrocenium Reduction on Highly Oriented Pyrolytic Graphite, *J. Electrochem. Soc.* 159 (2012) A1922-A1927.
- [20] P.A. Nelson, K.G. Gallagher, I. Bloom, D.W. Dees, Modeling the Performance and Cost of Lithium-Ion Batteries for Electric-Drive Vehicles, Argonne National Laboratory, 2012.
- [21] J. Ma, L. Seidl, W. Ju, E. Mostafa, L. Asen, S. Martens, U. Stimming, O. Schneider, Applications of Ionic Liquids in Electrochemical Energy Conversion and Storage, *ECS Transactions* 64 (2014) 407–423.
- [22] E. Markevich, M.D. Levi, D. Aurbach, New Insight into Studies of the Cycling Performance of Li-Graphite Electrodes A Combination of Cyclic Voltammetry, Electrochemical Impedance, and Differential Self-Discharge Measurements, *J. Electrochem. Soc.* 152 (2005) A778-A786.
- [23] M.D. Levi, C. Wang, D. Aurbach, Self-discharge of graphite electrodes at elevated temperatures studied by CV and electrochemical impedance spectroscopy, *J. Electrochem. Soc.* 151 (2004) A781-A790.
- [24] H. Matsuda, Y. Ayabe, Zur Theorie der Randles-Sevčičsches Kathodenstrahl-Polarographie, *Zeitschrift für Elektrochemie, Berichte der Bunsengesellschaft für physikalische Chemie* 59 (1955) 494–503.

- [25] H. Ota, Y. Sakata, A. Inoue, S. Yamaguchi, Analysis of vinylene carbonate derived SEI layers on graphite anode, *J. Electrochem. Soc.* 151 (2004) A1659-A1669.
- [26] J.-K. Park (Ed.), *Principles and Applications of Lithium Secondary Batteries*, 1st ed., Wiley-VCH Verlag GmbH & Co. KGaA, 2012.
- [27] H. Ota, K. Shima, M. Ue, J.-i. Yamaki, Effect of vinylene carbonate as additive to electrolyte for lithium metal anode, *Electrochimica Acta* 49 (2004) 565–572.
- [28] G. Amatucci, A. Du Pasquier, A. Blyr, T. Zheng, J.-M. Tarascon, The elevated temperature performance of the LiMn₂O₄/C system: failure and solutions, *Electrochimica Acta* 45 (1999) 255–271.
- [29] F.-M. Wang, H.-Y. Wang, M.-H. Yu, Y.-J. Hsiao, Y. Tsai, Differential pulse effects of solid electrolyte interface formation for improving performance on high-power lithium ion battery, *Journal of Power Sources* 196 (2011) 10395–10400.
- [30] L. Guo, P.C. Searson, On the influence of the nucleation overpotential on island growth in electrodeposition, *Electrochimica Acta* 55 (2010) 4086–4091.
- [31] A. Rinaldi, O. Wijaya, H. Hoster, Lithium-Oxygen Cells, *ChemElectroChem* 3 (2016) 1944–1950.
- [32] H.-J. Noh, Z. Chen, C.S. Yoon, J. Lu, K. Amine, Y.-K. Sun, Cathode Material with Nanorod Structure—An Application for Advanced High-Energy and Safe Lithium Batteries, *Chem. Mater.* 25 (2013) 2109–2115.
- [33] H.-J. Noh, J.W. Ju, Y.-K. Sun, Comparison of nanorod-structured Li[Ni_{0.54} Co_{0.16} Mn_{0.30}]O₂ with conventional cathode materials for Li-ion batteries, *ChemSusChem* 7 (2014) 245–252.
- [34] D. Andre, S.-J. Kim, P. Lamp, S.F. Lux, F. Maglia, O. Paschos, B. Stiaszny, Future generations of cathode materials: an automotive industry perspective, *J. Mater. Chem. A* (2015) 6709–6732.
- [35] C. Julien, Z. Stoyanov, *Materials for Lithium-Ion Batteries*, Springer Netherlands; Imprint; Springer, Dordrecht, 2000.
- [36] P.B. Balbuena, Y. Wang, *Lithium-ion batteries: Solid-electrolyte interphase*, Imperial College Press, London, 2004.
- [37] R.T. Jow, K. Xu, O. Borodin, M. Ue (Eds.), *Electrolytes for Lithium and Lithium-Ion Batteries*, Springer, New York, 2014.
- [38] B. Zhang, M. Metzger, S. Solchenbach, M. Payne, S. Meini, H.A. Gasteiger, A. Garsuch, B.L. Lucht, Role of 1,3-Propane Sultone and Vinylene Carbonate in Solid Electrolyte Interface Formation and Gas Generation, *J. Phys. Chem. C* 119 (2015) 11337–11348.
- [39] E. Peled, D. Golodnitsky, G. Ardel, Advanced model for solid electrolyte interphase electrodes in liquid and polymer electrolytes, *J. Electrochem. Soc.* 144 (1997) L208-L210.
- [40] S. Bhattacharya, A.T. Alpas, Micromechanisms of solid electrolyte interphase formation on electrochemically cycled graphite electrodes in lithium-ion cells, *Carbon* 50 (2012) 5359–5371.
- [41] M. Park, X. Zhang, M. Chung, G.B. Less, A.M. Sastry, A review of conduction phenomena in Li-ion batteries, *Journal of Power Sources* 195 (2010) 7904–7929.